

Genetic U-Net: Automatically Designing Lightweight U-shaped CNN Architectures Using the Genetic Algorithm for Retinal Vessel Segmentation

Jiahong Wei Zhun Fan

Department of Electronic Engineering, Shantou University, Guangdong, 515063, China

Key Lab of Digital Signal and Image Processing of Guangdong Province, Guangdong, 515063, China

Email: 19jhwei@stu.edu.cn zfan@stu.edu.cn

Abstract—Many previous works based on deep learning for retinal vessel segmentation have achieved promising performance by manually designing U-shaped convolutional neural networks (CNNs). However, the manual design of these CNNs is time-consuming and requires extensive empirical knowledge. To address this problem, we propose a novel method using genetic algorithms (GAs) to automatically design a lightweight U-shaped CNN for retinal vessel segmentation, called Genetic U-Net. Here we first design a special search space containing the structure of U-Net and its corresponding operations, and then use genetic algorithm to search for superior architectures in this search space. Experimental results show that the proposed method outperforms the existing methods on three public datasets, DRIVE, CHASE_DB1 and STARE. In addition, the architectures obtained by the proposed method are more lightweight but accurate than the state-of-the-art models.

Index Terms—Convolutional neural networks (CNNs), Genetic algorithms (GAs), Retinal vessel segmentation, Neural architecture search (NAS)

I. INTRODUCTION

The retinal vascular system is the only human blood vascular system that can be observed noninvasively in vivo [1] [2]. In addition, changes in the vasculature are often associated with certain diseases, so ophthalmologists and other doctors consider the fundus examination as a routine clinical examination [3]. Through the observation of the retinal vascular system, many diseases can be diagnosed and tracked [1]. The pathological changes of retinal vessels can reflect either ophthalmology diseases or other systemic diseases, such as wet age-related macular degeneration and diabetes. Diabetic retinopathy can lead to the growth of new blood vessels and wet age-related macular degeneration can cause the narrowing of blood vessels because of atherosclerosis [4] [5]. Moreover, the retinal vascular system of each eye is unique. without pathological changes, it does not alter throughout the lifetime. Therefore, observation of the retinal vascular system can also be applied in biometrics [6] [7]. No matter for the early detection of diseases or biometrics, retinal vessel segmentation is a prerequisite step for quantitative analysis. Through the retinal vessel segmentation, the relevant morphological information of retinal vascular tree (such as the width, length, and curvature

of blood vessels, etc.) can be obtained [8]. As a result, accurate segmentation of retinal vessels is of great significance.

However, due to the complicated situations in the fundus images, the automatic segmentation of retinal vessels is a challenging task. In the fundus images, the retinal vessels are difficult to be distinguished from the background because of the subtle difference between the vascular region and the background. The structure of the vascular tree is also complicated, with lots of cross-connected vessels and tiny vessels. Additionally, there are other factors that make segmentation difficult, such as pathological exudates and uneven illumination. Compared with the methods based on traditional image processing, the methods based on deep convolutional neural network demonstrate certain advantages on dealing with these complicated situations. In particular, after U-Net [9] was proposed, U-Net and its variants [10] [8] [11] [12] become the mainstream of retinal vessel segmentation. However, these U-Net based models still have some limitations in capturing vascular trees under complicated situations of the fundus images. Moreover, these hand-designed U-Net based models usually have high computational complexity and memory cost, which means that they cannot be run on devices without enough computing power. With the surging interests in neural architecture search (NAS), designing neural network architectures automatically for retinal vessel segmentation to find the lightweight neural architectures with yet competitive performance is undoubtedly desirable and even necessary.

In this paper, we propose an architecture search scheme combining genetic algorithm (GA) and U-Net, named Genetic U-Net, for retinal vessel segmentation. As we know, the reason that U-Net and its variants perform well in segmentation tasks is closely related to the following two main traits of U-Net: (1) U-shaped encoder-decoder structure; (2) Fusing features between encoder and decoder by skip connections. Based on this prior knowledge, we propose a condensed search space with architectures that can be optimized by the genetic algorithms (GAs). Genetic U-Net can design architectures much smaller but performing better than that of U-Net. The main contributions of the work include the following:

- We propose a novel automatic design method for U-shaped CNN architecture based on GA, especially for retinal vessel segmentation, which helps us to acquire high performing and transferable network architectures.

- We divide the U-shaped encoder-decoder structure into different blocks and then search flexibly for each block in a given search space using GA to automatically design the architectures with good performance without any manual processing.
- Through the observation and analysis of the searched architectures, we find that some patterns and operations that can well improve the performance of retinal vessel segmentation, which are unknown before.
- Compared with state-of-the-art models, the searched models achieve the best performance on several public datasets with the least amounts of parameters (weights).

II. RELATED WORK

A. Retinal Vessel Segmentation

Retinal vessel segmentation belongs to binary segmentation and is a subcategory of semantic segmentation. Due to the excellent effects of FCN [13] and U-Net [9] on image segmentation, fully convolutional neural networks have become mainstream for this task. Recently, the new state-of-the-art methods [14] [8] [15] [11] [16] [17] for retinal vessel segmentation are dominated by deep learning models, especially variants of U-Net.

Ref. [17] adds pre-trained components of MobileNetV2 [18] as the encoder and introduces novel contractive bottleneck blocks as the decoder, which achieves better performance, less computational cost, and faster inference speed. The encoder architecture used in this work is pre-trained on ImageNet [19], which is different from other methods. In [14], a joint-loss is adopted to provide supervision information for U-Net, with two branches responsible for pixel-wise loss and segment-level loss, respectively. The joint-loss can improve the capability of the model to balance segmentation of thick and thin vessels. [8] replaces traditional convolution with deformable convolution in U-Net to better capture the miscellaneous morphology of vascular trees. [15] designs a novel inception-residual block and introduces four supervision paths with different kernel sizes of convolution to utilize multi-scale features. [16] embeds dense dilated convolutional blocks between the same level encoder and decoder cells, and uses regularized walk algorithm to post-process model predictions. The model in [11] has two encoders based on U-Net. One encoder path is for extracting spatial information and the other path is for extracting context information. A novel module is also used to combine the information of the two paths.

B. Neural Architecture Search

According to optimization methods, there are three main categories of neural architecture search: reinforcement learning based, evolutionary algorithm based, and differentiable architecture search. The methods based on reinforcement learning [20] [21] [22] formulate NAS as a Markov decision process. A controller is used to sample the architectures and learn to generate better and better architectures from continuous trial and error, with the performance of these architectures as reward feedback. The methods based on evolutionary algorithms [23] [24] formulate NAS as an optimization problem and encode

the architectures. More competitive architectures are generated by applying some genetic operations (e.g., crossover, and mutation) and will be kept as offsprings in the next generation. Generation after generation, the architectures are continuously optimized until architectures with satisfactory performances are obtained. For differentiable neural architecture search [25] [26], each operation option is assigned a weight coefficient. The parameter weights of the architecture and the weights of the operation options are optimized alternatively by gradient descent. The optimal architecture is usually obtained by selecting the operation with the largest weight after convergence.

Neural architecture search (NAS) not only has achieved great success in image recognition, but there are many recent works that extend NAS to the image segmentation [27] [28] and object detection [29] [30] [31], including some works applying NAS to medical image segmentation. [32], [33] and [34] are mainly to optimize the hyperparameters and operations of each layer of the building blocks, but the topology of the block is relatively fixed. [35] and [36] optimize the structure and operations of one or two types of building blocks, then compose the architecture by stacking them repeatedly. However, in our work, the topology and operations of each block can be different and optimized flexibly at the same time.

III. THE PROPOSED METHOD

In this section, we present the proposed method in detail. We first introduce the search space of the architectures, then explain the method of encoding an architecture into a binary string, and finally explain the genetic algorithm with some operations (e.g., crossover, mutation and selection) searching competitive architectures.

A. The search space and encoding

1) *Backbone of the Search Space*: As shown in Fig. 1(a), U-Net is a symmetrical CNN architecture, which is composed of an encoder E and a decoder D . Both encoder E and decoder D contain several blocks, such as e_i ($i = 0, 1, 2, 3$) and d_j ($j = 0, 1, 2$). From top to bottom, U-Net is divided into different stages S_k ($k = 0, 1, 2, 3$) and feature dimensions are constant in the same stage. Except for the last stage, skip connections are adopted in all other stages to provide features with different semantic information extracted by the encoder to the decoder, which can not only strengthen the connection between encoder and decoder but also alleviate vanishing gradient problem [37] [38] in model training.

Decoder D needs to fuse features from skip connections and up-sampling, and there are two commonly used feature fusion operations: concatenation or element-wise addition. Although original U-Net employs concatenation for feature fusion, some U-Net variants [39] can achieve good results by using element-wise addition. Fig. 1(b) clearly illustrates their main difference. Compared with element-wise addition, concatenation generates larger feature maps which will increase computational complexity. To mitigate the computational complexity, we select addition operation for feature fusion in this paper.

On the one hand, applying too large a search space will increase the difficulty of the architecture search. It is more

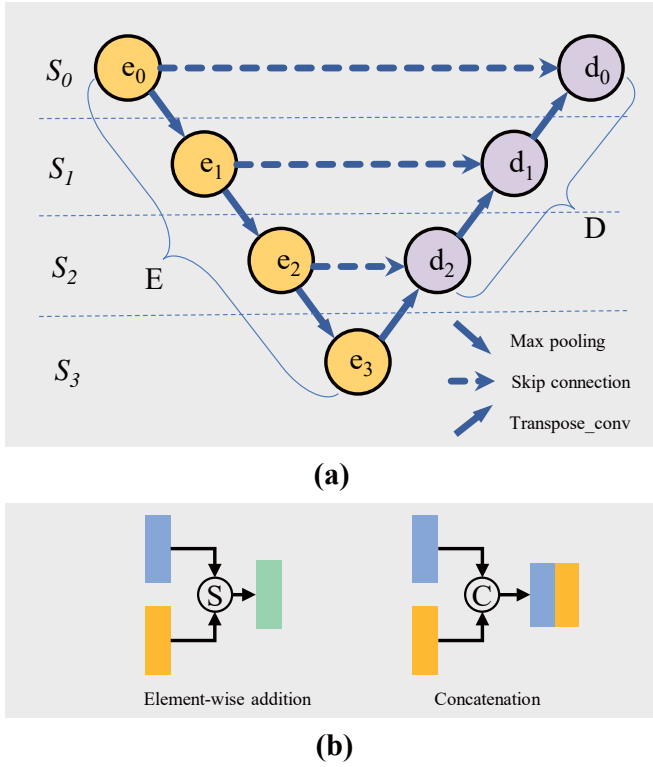


Fig. 1. (a) The backbone of U-Net; (b) Two operations for feature fusion.

likely that after a long-term search, the results are still unsatisfactory. On the other hand, applying too small a search space will limit the architecture flexibility, making it difficult to get promising architectures, too. If a reasonably condensed search space can be set up based on some prior knowledge, it will enable the algorithm to find optimal architectures more efficiently without loss of the architectural flexibility.

The successful applications of U-Net and its variants reveal that the U-shaped encoder-decoder structure has strong applicability, which is valuable prior knowledge for our design of the search space. Therefore, in this paper, we use the U-shaped decoder-encoder structure as the backbone which consists of several different building blocks. We can then search for satisfactory architectures via adjusting their internal structures of the these building blocks. The adopted U-shaped structure with seven blocks and four stages is shown in Fig. 1(a). In general, fewer stages mean smaller models with fewer blocks, which for certain tasks may lead to poor performance because the depth of the model is not enough. More stages correspond to deeper models and larger search space, which on the other hand may lead to lower search efficiency and higher computational cost, even though potentially better models may be found in an enlarged search space. A compromise has to be made in order to search for a sufficiently small model with yet a satisfactory performance.

2) *The Building Blocks and Their Encoding*: In original U-Net, the internal structure of each block is composed of two basic layers (3×3 Conv + ReLU). Usually, the U-Net variants [40] [41] [10] improve their performance by adjusting the internal structure of blocks (e.g., ResNet block [42], DenseNet

block [43] and InceptionNet block [44]), which illustrates the importance of the internal structures of blocks.

The internal structures of the building blocks are represented in the same way as in Genetic CNN [23], so we do not explain it in detail here and some details could be referred in [23]. The internal structure of each block is a directed acyclic graph consisting of some edges and nodes. Each node represents an operation unit or an operation sequence, and each edge represents the connection between nodes. A directed edge of two nodes is to transform the output feature map of the pre-node to the post-node. Fig. 2 shows two examples of connections between nodes in a block, and the numbers in nodes just indicate their orders. Genetic CNN uses binary encoding to represent the connections between nodes, and all nodes are with a solid operation sequence or an operation (e.g., 3×3 Conv + BN + ReLU or 3×3 Conv). In our work,

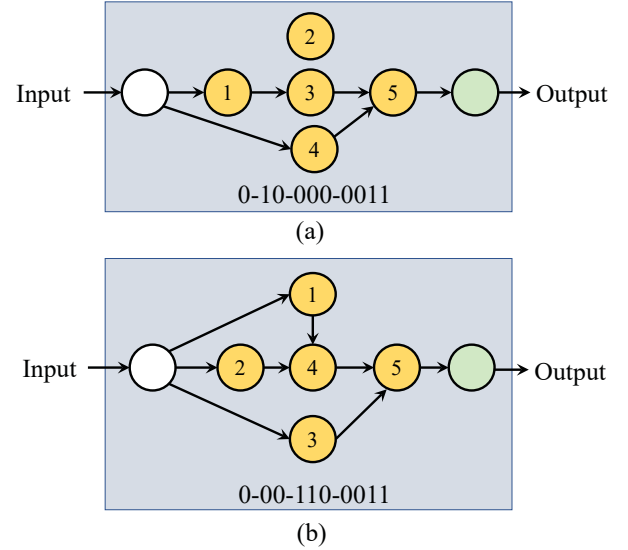


Fig. 2. Two encoding examples of block.

sixteen operation sequences shown in Table I are provided as options for the nodes. We search for the optimal structure and operation of the blocks at the same time. Each operation sequence has its unique ID and consists of some basic operation units which include 3×3 Conv, 5×5 Conv, ReLU [45], Mish [46] and instance normalization [47]. The basic operation units do not include batch normalization [48] because the batch size is set as 1, in which case using batch normalization is unnecessary. These operation units are some commonly used operations of CNNs in the machine learning community and our purpose is to find the most useful operation sequence for retinal vessel segmentation. The differences between these operation sequences are reflected in the convolutional kernel size, activation functions, activation types (pre-activation or post-activation), and normalization types (whether instance normalization is utilized), so the binary encoding with four bits is utilized for representing these operation sequences. We assume that the nodes in the same block have the same operation sequence, so each block gene is composed of an operation gene with four bits and a connection gene (Shown

in Fig. 3(a)). Besides, seven block genes together constitute the genotype of an architecture (Shown in Fig. 3(b)).

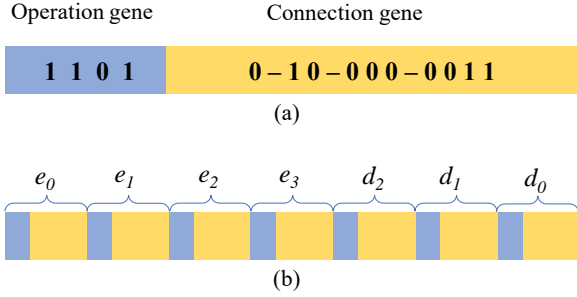


Fig. 3. (a) A block gene; (b) Genotype of an architecture.

TABLE I
THE OPERATION SEQUENCES FOR THE NODES. IN IS THE INSTANCE
NORMALIZATION.

ID	Operation sequence
0	$3 \times 3 \text{ Conv} \rightarrow \text{ReLU}$
1	$3 \times 3 \text{ Conv} \rightarrow \text{Mish}$
2	$3 \times 3 \text{ Conv} \rightarrow \text{IN} \rightarrow \text{ReLU}$
3	$3 \times 3 \text{ Conv} \rightarrow \text{IN} \rightarrow \text{Mish}$
4	$5 \times 5 \text{ Conv} \rightarrow \text{ReLU}$
5	$5 \times 5 \text{ Conv} \rightarrow \text{Mish}$
6	$5 \times 5 \text{ Conv} \rightarrow \text{IN} \rightarrow \text{ReLU}$
7	$5 \times 5 \text{ Conv} \rightarrow \text{IN} \rightarrow \text{Mish}$
8	$\text{ReLU} \rightarrow 3 \times 3 \text{ Conv}$
9	$\text{Mish} \rightarrow 3 \times 3 \text{ Conv}$
10	$\text{IN} \rightarrow \text{ReLU} \rightarrow 3 \times 3 \text{ Conv}$
11	$\text{IN} \rightarrow \text{Mish} \rightarrow 3 \times 3 \text{ Conv}$
12	$\text{ReLU} \rightarrow 5 \times 5 \text{ Conv}$
13	$\text{Mish} \rightarrow 5 \times 5 \text{ Conv}$
14	$\text{IN} \rightarrow \text{ReLU} \rightarrow 5 \times 5 \text{ Conv}$
15	$\text{IN} \rightarrow \text{Mish} \rightarrow 5 \times 5 \text{ Conv}$

In Genetic CNN, the default input node and default output node (Marked white and green in Fig. 2, respectively) process the aggregated information linearly by using a $3 \times 3 \text{ Conv}$ operation, which has limitations compared with the nonlinear processing, so we make these two nodes take the same operation sequence with an activation function as other nodes in our work.

It is also worth noting that our approach is different from Genetic CNN, even though the use of blocks has some similarities. Two main differences can be summarized as (1) Genetic CNN is applied to image classification while the proposed method is applied to image segmentation; (2) The U-shaped encoder-decoder structure is employed as the backbone in our work while it is not employed as the backbone in Genetic CNN.

B. Evolutionary Algorithm

Genetic U-Net follows an iterative evolutionary process to generate a continuously improved population. In the population, each individual stands for an architecture, and its fitness

depends on the performance of the corresponding architecture in particular applications. The flowchart of Genetic U-Net is summarized in Algorithm 1. It starts with a randomly initialized population with N individuals. Following initialization, we evolve T generations, each of which contains three evolutionary operations (e.g., crossover, mutation and selection). After the new individuals are generated, we evaluate them via training the architectures they encode from scratch on the provided dataset.

Algorithm 1: Framework of the Proposed Method

Input: The population size N , the maximal generation number T , the crossover probability p_c , the mutation probability p_m , the mutation probability p_b of each bit.

Output: The discovered best architectures.

- 1 $P_0 \leftarrow$ Initialize a population with the size of N by using the binary encoding strategy;
- 2 Evaluate the fitness of individuals in P_0 ;
- 3 **while** $t \leftarrow 0 < T$ **do**
- 4 $Q_t \leftarrow \emptyset$;
- 5 **while** $|Q_t| < N$ **do**
- 6 $p_1, p_2 \leftarrow$ Select two parent individuals from P_t ;
- 7 $q_1, q_2 \leftarrow$ Generate two offspring p_1 and p_2 by crossover operation with the probability p_c and mutation with the probability p_m and p_b ;
- 8 $Q_t \leftarrow Q_t \cup q_1 \cup q_2$;
- 9 **end**
- 10 Evaluate the fitness of individuals in Q_t ;
- 11 $P_{t+1} \leftarrow$ Select N individuals from $P_t \cup Q_t$ by environmental selection;
- 12 $t \leftarrow t + 1$;
- 13 **end**
- 14 **return** the individuals with the best fitness in P_t .

1) *Crossover Operation:* Crossover is to exchange information between individuals, and effective information exchange can ensure the convergence of the algorithm. In traditional GAs, one-point crossover or two-point crossover is usually used for generating offspring, but these two types of crossover with small search step size often result in a less impressive performance, especially for genes with long length. GAs with a large search step size are better than GAs with a small step size for most problems [49], so multi-point crossover with a large search step size is adopted for the algorithm. Besides, if two parent individuals are similar, the crossover between them may make little difference and even slow down the evolutionary process. After crossover, if the generated offspring individuals are very similar to the parent individuals, it may mean that this crossover does not function effectively. To relieve this problem, we design a method named *difference-guided* to choose two relatively different parent individuals for crossover. In the beginning, two individuals p_1 and p_2 are chosen by binary tournament selection [50]. Here, binary tournament selection is utilized to better retain the population diversity. Next, the difference *diff* between p_1 and p_2 is calculated by

Eq. (1). If $diff$ is larger than the threshold μ , p_1 and p_2 are designated as parents. If not, p_1 and p_2 will be reselected in the same way. If ten re-selections of p_1 and p_2 do not meet the requirement, the last selection will be designated as parents. After that, the designated parents will mate with the probability p_c . Algorithm 2 shows the details of the crossover operation in the proposed algorithm.

The difference between two individuals can be formalized as:

$$diff = \frac{sum(XOR(p_1, p_2))}{L_{gene}} \in [0, 1] \quad (1)$$

Where sum denotes summation function, and XOR denotes xor operation. p_1 and p_2 are two individuals to mate, and L_{gene} is the length of an individual gene.

Algorithm 2: Difference-guided Crossover Operation

Input: The population P_t , the probability for crossover operation p_c , the difference threshold of crossover operation μ .

Output: Two offsprings o_1, o_2 .

```

1  $o_1, o_2 \leftarrow \emptyset$ 
2 while  $j \leftarrow 0 < 10$  do
3    $p_1 \leftarrow$  Randomly select two individuals from  $P_t$ ,
   and from the two select the one with better
   fitness;
4    $p_2 \leftarrow$  Repeat Line 3;
5    $diff \leftarrow$  Compute the difference between  $p_1$  and
    $p_2$ ;
6   if  $diff > \mu$  then
7     break;
8   end
9    $j \leftarrow j + 1$ ;
10 end
11  $r \leftarrow$  Randomly generate a number from (0, 1);
12 if  $r < p_c$  then
13    $len \leftarrow$  Compute the length of  $p_1$  and  $p_2$ ;
14    $ints \leftarrow$  Randomly choose ten different integers
   from  $[0, len)$  and sort them;
15    $(i_0, i_1), (i_2, i_3), (i_4, i_5), (i_6, i_7), (i_8, i_9) \leftarrow$  Divide
    $ints$  into five pairs in order;
16   while  $k \leftarrow 0 < 5$  do
17      $p_1, p_2 \leftarrow$  Exchange  $p_1[i_{2k} : i_{2k+1}]$  and
      $p_2[i_{2k} : i_{2k+1}]$ ;
18   end
19    $o_1, o_2 \leftarrow p_1, p_2$ ;
20 else
21    $o_1, o_2 \leftarrow p_1, p_2$ ;
22 end
23 return  $o_1, o_2$ .
```

2) *Mutation*: Mutation can keep population diversity and prevent the algorithm from trapping in a local optimum. In the proposed method, the offspring generated via crossover are with the probability p_m to mutate and each bit is with the probability p_b to flip independently. p_b is a relatively small value (e.g., 0.05), so that an individual will not be changed too much after mutation, which is to say that mutation would

preserves the favorable properties of the surviving individuals while increasing the possibility of generating better offspring.

3) *Environmental Selection*: Typically, GAs select the next population by tournament selection or roulette selection. Both selections may miss the best individuals, resulting in the performance of the population degrading, even they maintain the population diversity [51]. On the other hand, if we explicitly select the best individuals for the next generation, a premature phenomenon [52] [53] may be caused and make the algorithm trap into local optimum [54] because of the loss of population diversity. Hence, when choosing the next population, both the best individuals and the relatively poor individuals should be selected, which can give consideration to both the convergence of the algorithm and the population diversity.

Algorithm 3: Environmental Selection

Input: The parent population P_t , the offspring population Q_t .

Output: The population for the next generation P_{t+1} .

```

1  $P_{t+1} \leftarrow \emptyset$ ;
2  $P_{best} \leftarrow$  Select the best five individuals from  $P_t \cup Q_t$ ;
3  $P_t \cup Q_t \leftarrow$  Remove  $P_{best}$  from  $P_t \cup Q_t$ ;
4  $P_{t+1} \leftarrow P_t \cup P_{best}$ ;
5 while  $|P_{t+1}| < |P_t|$  do
6    $p_1, p_2 \leftarrow$  Randomly select two individuals from
    $P_t \cup Q_t$ ;
7    $p \leftarrow$  Select the one who has a better fitness from
    $\{p_1, p_2\}$ ;
8    $P_{t+1} \leftarrow P_{t+1} \cup p$ ;
9 end
10 return  $P_{t+1}$ .
```

Algorithm 3 shows the process of environmental selection for the algorithm. First, given the current population P_t and the generated offspring population Q_t , the top five best individuals are selected into the next population P_{t+1} and removed from $P_t \cup Q_t$. Second, $|P_t| - 5$ individuals are selected from $P_t \cup Q_t$ by using the binary tournament selection, and then these $|P_t| - 5$ selected individuals are placed into P_{t+1} . At this time, the size of the next population P_{t+1} is kept the same as the size of the current population P_t .

4) *Fitness Evaluation*: In Genetic U-Net, the fitness of an individual is the *F1-score* (as explained in section IV-C) based on the architecture the individual represents and the data for validation, because the *F1-score* is a comprehensive metric for retinal vessel segmentation that can deal with the imbalance problem of samples. Algorithm 4 summarizes the procedure of evaluating the individuals of the population. For evaluation, each individual has to transform itself into the architecture, which is an inverse process of binary encoding. Before training, He initialization [55] is used to initialize the weights of the architecture. Then, on the training data, the architecture is trained by Lookahead [56] which uses Adam [57] as the base optimizer. After 80 epochs of training, the validation data is used to validate the trained architecture at the end of each epoch until 130th epoch, and the best *F1-score* during this process is set as the fitness of the corresponding individual.

The architectures are not trained to converge, but adopt the early stop strategy. Under the early stop, the performance of the architectures can still be accurately evaluated with less evaluation time.

Algorithm 4: Evaluate Fitness

Input: The population P_t for fitness evaluation, training data D_{train} , validation data D_{valid} .
Output: The population P_t with fitness.

- 1 **foreach** *individual* in P_t **do**
- 2 $arch \leftarrow$ Transform the *individual* to its corresponding architecture;
- 3 Apply weight initialization to $arch$;
- 4 $epoch \leftarrow 0$;
- 5 $F1 - score_{best} \leftarrow 0$;
- 6 **for** $epoch < 130$ **do**
- 7 Train $arch$ on D_{train} by gradient descent for an epoch;
- 8 **if** $epoch > 80$ **then**
- 9 $F1 - score \leftarrow$ Evaluate the trained $arch$ on D_{valid} ;
- 10 **if** $F1 - score > F1 - score_{best}$ **then**
- 11 $F1 - score_{best} \leftarrow F1 - score$;
- 12 **end**
- 13 **end**
- 14 **end**
- 15 Set $F1 - score_{best}$ as the fitness of *individual*;
- 16 **end**
- 17 **return** P_t .

IV. MATERIALS FOR EXPERIMENTS

A. Loss Function

In fundus images, the ratio of vessel pixels is less than 0.1, and most of the pixels belong to non-vessel. The problem of imbalanced samples needs to be dealt with. For this purpose, focal loss [58] originally proposed to alleviate the sample imbalance problem in object detection is utilized as loss function in this work, which is given in Eq. (2), where y , \hat{y} , n , m indicate ground truth, model prediction, n th sample, and the total number of samples, respectively.

$$Loss = - \sum_{n=1}^m (\alpha y_n (1 - \hat{y}_n)^\omega \log \hat{y}_n + (1 - \alpha) (1 - y_n) \hat{y}_n^\omega \log (1 - \hat{y}_n)) \quad (2)$$

B. Datasets

Three public datasets DRIVE [59], CHASE_DB1 [60] and STARE [61] are used in our experiments. Some descriptions and examples of these datasets are given in Table II and Fig. 4, respectively.

Each dataset has two different annotations from two experts, and we only take the annotations of the first expert as the ground truth in our experiments. For the split of training and test datasets, we adopt the same way as in [10] [62] [63].

TABLE II
DESCRIPTIONS OF THE DATASETS.

Dataset	Year	Quantity	Resolution
DRIVE	2000	40	565×584
STARE	2004	20	700×605
CHASE_DB1	2012	28	999×960

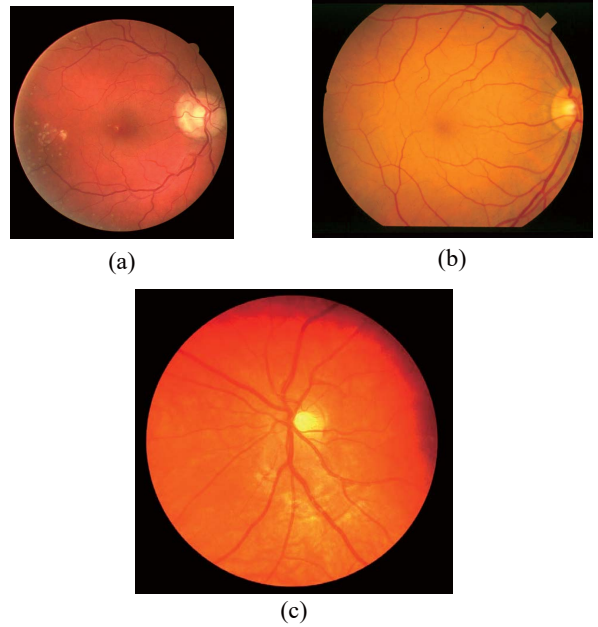


Fig. 4. Examples of dataset images (HxW). (a): DRIVE (584x565); (b): STARE (700x605); (c): CHASE_DB1 (999x960).

C. Evaluation Metrics

Retinal vessel segmentation is a binary classification problem, which classifies each pixel in the fundus image as vessel or non-vessel. The output of the model is a probability map which gives the probability to each pixel belonging to the class of vessels, and the probability threshold is set to 0.5 to get the final results in our work. If a vessel pixel is correctly classified, it is a true positive (TP); if not, it is a false positive (FP). If a non-vessel pixel is precisely classified, it is a true negative (TN); if not, it is a false negative (FN). As shown in Table III, five metrics are selected for evaluation.

TABLE III
METRICS FOR EVALUATION IN OUR WORK.

Metrics	Description
ACC (<i>accuracy</i>)	$ACC = (TP + TN) / (TP + TN + FP + FN)$
SE (<i>sensitivity</i>)	$SE = TP / (TP + FN)$
SP (<i>specificity</i>)	$SP = TN / (TN + FP)$
$F1$ -score ($F1$)	$F1 = (2 \times TP) / (2 \times TP + FP + FN)$
$AUROC$	Area Under the ROC curve.

V. EXPERIMENTS

The experiments in this paper include two stages. The first stage is the architecture search stage, and the second is the architecture validation stage. In the first stage, the neural architectures are searched by GA until the algorithm converges. In the second stage, the searched architectures are trained from scratch (validated) to get their performances on retinal vessel segmentation. In this section, we will introduce these two stages of the experiments and analyze their results.

A. Experimental Setup

Dataset for searching: In the architecture search stage, a subset of the trainset is selected for validation, and there is no access to the test set. The reason for that is to keep the experimental objectivity in the architecture validation stage. We will search the architectures on DRIVE. The last five images of its trainset are selected for validation while the rest fifteen images are for training. We will also transfer the architectures searched on DRIVE to other datasets (STARE and CHASE_DB1) in the architecture validation stage.

Genetic U-Net hyper-parameters: The number of nodes in each block is set to 5 by default (except for the input and output nodes). To keep the architecture compact, the number of channels of convolution operations inside the nodes is set to a relatively small value, 20. The up-sampling and down-sampling operations are the same as the original U-net. Max pooling with kernel size of 2 and stride of 2 is used for down-sampling, and transpose convolution with kernel size of 2 and stride of 2 is for up-sampling. The probability of crossover and mutation operations (p_c and p_m) is set to 0.9 and 0.7 respectively, and the difference threshold μ is set to 0.2. During mutation, the probability p_b is 0.05. The population size N is 20, the number of the generations T is 50, and 1000 candidates are generated during the search, meaning 1000 architectures are evaluated.

Network training during search: For data argumentation, horizontal flip, vertical flip, and random rotation from $[0^\circ, 360^\circ]$ are employed to increase the training data, which prevents the models from overfitting. The pixels of the images are normalized to $[-0.5, 0.5]$. We take the full image as the input instead of the patches, and the batch size is 1. For the optimizer, Lookahead [56] and Adam [57] take the default parameters (e.g., $\alpha = 0.5$, $k = 6$, $\beta_1 = 0.9$, $\beta_2 = 0.999$). The learning rate is initialized as 0.001. The architectures are trained on two NVIDIA TITAN RTX GPUs implemented in PyTorch 1.5.0. Ten neural architectures can be trained on two GPUs in parallel, which takes about 30 minutes to evaluate all individuals of one generation.

Network training after search: In the architecture validation stage, the settings of training are basically the same as the architecture search stage (e.g., optimizer, loss function, and data argumentation). The main difference is that the number of training epoch is expanded to 900, which is to ensure the convergence of the training. The data-split follows the way described in section IV-B.

B. Experimental Results of the Searched Model

1) *Comparison with Existing Methods:* We report the test results of the searched architecture (searched on DRIVE) on three public datasets (DRIVE, STARE, and CHASE_DB1) and compare them with other existing deep learning based methods.

Our results are summarized in Tables IV, V, and VI. The results of the existing methods are gained from their original papers. For fairness, our method has the same data-split as other methods. As we can see, our method almost dominates all the existing methods on the five chosen metrics, which means that the searched architecture achieves the best overall performance. More importantly, two comprehensive metrics *FI-score* and *AUROC* are better than other methods with a certain margin. Only a few simple data argumentations are utilized in our work, such as flip and rotation. The data argumentations in our methods are relatively simpler and less diverse than other methods, but we are still able to obtain superior results because of the excellence of the searched architecture. Besides, the searched architecture searched on DRIVE also successfully transfer to the other two datasets STARE and CHASE_DB1.

2) *Comparison with the Original U-Net:* Because our work uses the U-shaped encoder-decoder structure as the backbone based on the original U-Net [9] which can be regarded as the baseline of our work, we comprehensively compare the searched model with the original U-Net.

For a fair comparison, we train the original U-Net under the same settings as the searched architecture. As Table VII illustrated, the searched architecture outperforms the original U-Net on all three datasets.

Also, we present some examples of the results in Fig. 5 and Fig. 6. It can be seen that the searched architecture can accurately segment retinal vessels and the segmented structure is complete. Thick, thin, and cross-connected vessels can be segmented, even if there are inhomogeneous illumination and some exudates. However, the original U-Net cannot do well in these situations. The blue pixels in the images indicate false negative, which is from the vessel regions not detected. As we can see, there are more blue pixels in the results of the original U-Net, either from the overall view or from the locally magnified view. It can be further observed that the original U-Net shows its limitations in extracting complicated structural features, while the searched architecture can extract them much better.

Moreover, we analyze the computational efficiency of the searched architecture. Based on Table VIII, the total number of parameters in the searched architecture is about 0.27 Million, which is a $115\times$ reduction compared to the 31.03 Million parameters in U-Net. To evaluate our models for inference, we measure execution time and model size on an NVIDIA TITAN RTX GPU by using the PyTorch 1.5.0. The model size of the searched architecture is 1.2 MB, which is consistent with the number of parameters and, as expected, is about $100\times$ reduction compared to 120MB of U-Net. The execution time and MACs result on DRIVE are obtained with an input dimension $3\times 565\times 584$. The total number of MACs in the searched model in one forward propagation is 41 Billion which

TABLE IV
COMPARISON WITH EXISTING METHODS ON DRIVE DATASET.

Methods	Year	ACC	SE	SP	FI	AUROC	Params(M)
Vega <i>et al.</i> [64]	2015	0.9412	0.7444	0.9612	0.6884	N/A	N/A
Li <i>et al.</i> [65]	2015	0.9527	0.7569	0.9816	N/A	0.9738	N/A
Fan <i>et al.</i> [66]	2016	0.9614	0.7191	0.9849	N/A	N/A	N/A
Fan and Mo [67]	2016	0.9612	0.7814	0.9788	N/A	N/A	N/A
Liskowski <i>et al.</i> [62]	2016	0.9535	0.7811	0.9807	N/A	0.979	48.00
Orlando <i>et al.</i> [63]	2016	N/A	0.7897	0.9684	0.7857	N/A	N/A
Mo and Zhang [68]	2017	0.9521	0.7779	0.9780	N/A	0.9782	N/A
Xiao <i>et al.</i> [12]	2018	0.9655	0.7715	N/A	N/A	N/A	N/A
Alom <i>et al.</i> [10]	2019	0.9556	0.7792	0.9813	0.8171	0.9784	1.07
Jin <i>et al.</i> [8]	2019	0.9566	0.7963	0.9800	0.8237	0.9802	0.88
Bo Wang <i>et al.</i> [11]	2019	0.9567	0.7940	0.9816	0.8270	0.9772	N/A
Mou Lei <i>et al.</i> [16]	2019	0.9594	0.8126	0.9788	N/A	0.9796	56.03
Yicheng Wu <i>et al.</i> [15]	2019	0.9578	0.8038	0.9802	N/A	0.9821	1.70
Genetic U-Net	2020	0.9707	0.8300	0.9843	0.8314	0.9885	0.27

TABLE V
COMPARISON WITH EXISTING METHODS ON STARE DATASET.

Methods	Year	ACC	SE	SP	FI	AUROC
Vega <i>et al.</i> [64]	2015	0.9483	0.7019	0.9671	0.6614	N/A
Li <i>et al.</i> [65]	2015	0.9628	0.7726	0.9844	N/A	0.9879
Fan <i>et al.</i> [66]	2016	0.9588	0.6996	0.9787	N/A	N/A
Fan and Mo [67]	2016	0.9654	0.7834	0.9799	N/A	N/A
Liskowski <i>et al.</i> [62]	2016	0.9729	0.8554	0.9862	N/A	0.9928
Orlando <i>et al.</i> [63]	2017	N/A	0.7680	0.9738	0.7644	N/A
Mo and Zhang [68]	2018	0.9674	0.8147	0.9844	N/A	0.9885
Xiao <i>et al.</i> [12]	2019	0.9693	0.7469	N/A	N/A	N/A
Alom <i>et al.</i> [10]	2019	0.9712	0.8292	0.9862	0.8475	0.9914
Jin <i>et al.</i> [8]	2019	0.9641	0.7595	0.9878	0.8143	0.9832
Genetic U-Net	2020	0.9792	0.8658	0.9886	0.8630	0.9942

TABLE VI
COMPARISON WITH EXISTING METHODS ON CHASE_DB1 DATASET.

Methods	Year	ACC	SE	SP	FI	AUROC
Li <i>et al.</i> [65]	2015	0.9527	0.7569	0.9816	N/A	0.9738
Fan and Mo [67]	2016	0.9573	0.7656	0.9704	N/A	N/A
Liskowski <i>et al.</i> [62]	2016	0.9628	0.7816	0.9836	N/A	0.9823
Orlando <i>et al.</i> [63]	2016	N/A	0.7277	0.9712	0.7332	N/A
Mo and Zhang [68]	2017	0.9581	0.7661	0.9793	N/A	0.9812
Alom <i>et al.</i> [10]	2019	0.9634	0.7756	0.9820	0.7928	0.9815
Jin <i>et al.</i> [8]	2019	0.9610	0.8155	0.9752	0.7883	0.9804
Bo Wang <i>et al.</i> [11]	2019	0.9661	0.8074	0.9821	0.8037	0.9812
Yicheng Wu <i>et al.</i> [15]	2019	0.9661	0.8132	0.9814	N/A	0.9860
Genetic U-Net	2020	0.9769	0.8463	0.9857	0.8223	0.9914

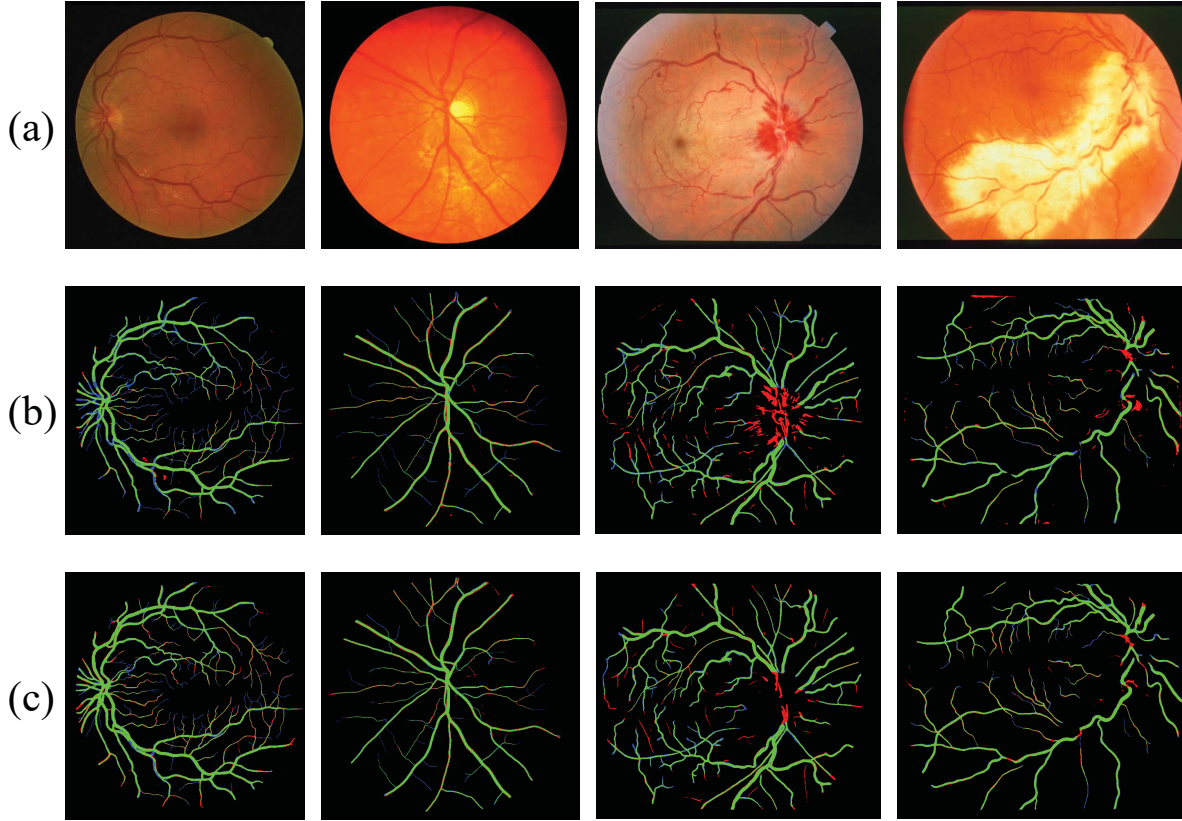


Fig. 5. Overall view visualization of the segmentation results. Green pixel indicates true positive, red pixel indicates false positive and blue pixel indicates false negative. (a) The Original Images; (b) The Results of U-Net; (c) The Results of Genetic U-Net.

TABLE VII
COMPARISON WITH U-NET ON THREE DATASETS.

Datasets	Models	ACC	SE	SP	F1	AUROC
DRIVE	U-Net	0.9690	0.8091	0.9846	0.8191	0.9863
	Genetic U-Net	0.9707	0.8300	0.9843	0.8314	0.9885
STARE	U-Net	0.9756	0.8187	0.9870	0.8273	0.9894
	Genetic U-Net	0.9792	0.8658	0.9886	0.8630	0.9942
CHASE_DB1	U-Net	0.9753	0.8298	0.9851	0.8092	0.9895
	Genetic U-Net	0.9769	0.8463	0.9857	0.8223	0.9914

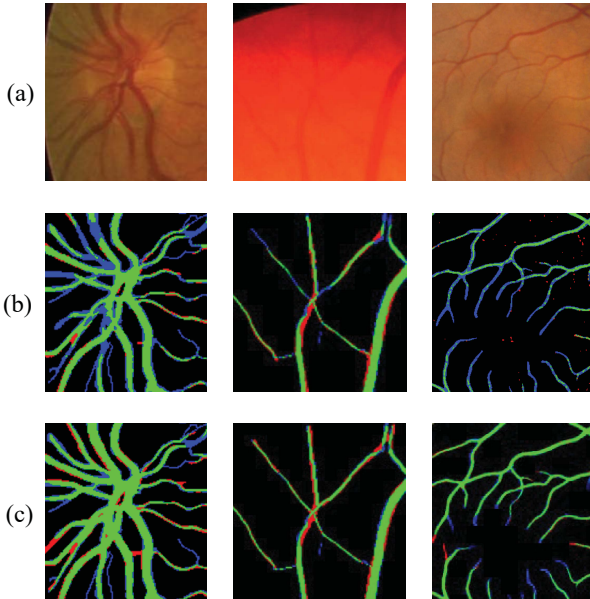


Fig. 6. Locally magnified view visualization of the segmentation results. (a) The Original Images; (b) The Results of U-Net; (c) The Results of Genetic U-Net.

is a $3.2\times$ reduction compared to the 142 Billion MACs in U-Net. For the execution time, the searched architecture also achieves about $1.3\times$ reduction compared to U-Net.

TABLE VIII
COMPARISON OF MODEL SIZE, PARAMETERS, MACS AND EXECUTION TIME WITH U-NET. THE MACS AND EXECUTION TIME ARE CALCULATED BASED ON AN INPUT SIZE OF $3\times 565\times 584$.

Models	Model size	Params	MACs	Exe time
U-Net	120 MB	31.03 M	142 B	35.4 ms
Genetic U-Net	1.2 MB	0.27 M	41 B	27.5 ms

C. Experimental Analysis of Architecture Search

The evolutionary trajectory is the blue line shown in Fig. 8. As we can see, the average fitness of the top five individuals gradually increase from the first generation and stop changing at about the 50th generation, which indicates that the algorithm converges. Thus, we terminate the architecture search after the 50th generation and select the best individual from the last population as the result. Fig. 9 displays the searched architecture decoded from the selected individual.

1) *Observations and Findings:* The final results of the evolutionary algorithm usually contain some useful information for us to further improve our work. In order to find some patterns for more efficient architecture design, we observe and analyze the top five architectures of the last generation.

Topology structure: We observe the topology inside each block of these architectures displayed in Appendix. Almost all these blocks have the allowed maximum number of nodes and their internal structure is relatively complex. There are quite a few skip connections between the nodes. In addition, all blocks have two or three parallel branches inside them, which look like InceptionNet [44] block.

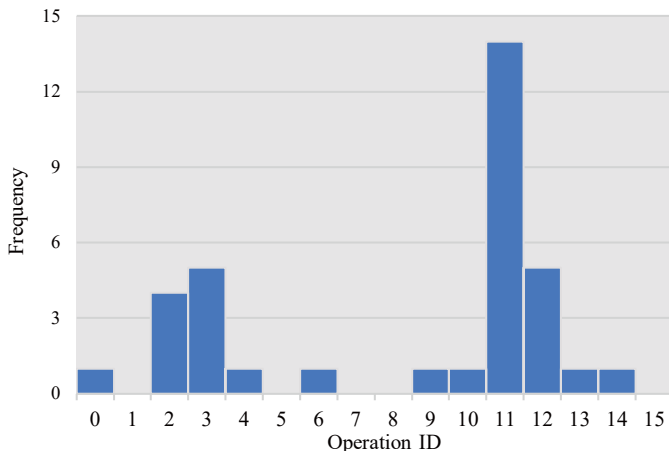


Fig. 7. Frequency of the operation sequences.

Operations and operation sequences: We obtain the statistics of the frequency of occurrence of all operation sequences listed in Table I. From Fig. 7, it is noticeable that the operation sequence with ID 11 has the highest frequency. To further verify the effect of this operation sequence, we use it to replace the basic convolutional layer ($3 \times 3 \text{ Conv} + \text{ReLU}$) of the U-Net [9] blocks and conduct experiments on DRIVE. The result is reported in the eighth row of Table IX. As expected, after U-Net uses this operation sequence, its performance of retinal vessel segmentation on DRIVE can be greatly improved. But surprisingly, its performance surpasses existing methods listed in Table IV, except the searched architecture using the proposed approach in this work. It is worthwhile to further explore the reasons why only changing some operations of U-Net blocks can lead to such a large improvement of its performance. After replacing the original basic convolution layer in U-Net with the operation sequence with ID 11, U-Net is with different activation function (Mish), different activation type (pre-activation), and instance normalization. These three

changes can boost the U-Net together. In order to find out which factor or factors will have a greater impact on U-Net, we do six additional sets of experiments on U-Net, with the results listed in the second to the seventh row in Table IX. From the data of the second to the fourth row, we can see that adding instance normalization or using pre-activation can improve the performance of U-Net to some extent. In particular, the effect of adding instance normalization is very obvious. U-Net is not improved just by changing the activation function into Mish. Furthermore, from the data of the fifth to the eighth row, it can also be seen that adding instance normalization or using pre-activation is useful to get better performance. When instance normalization and pre-activation are employed together, the effect is more obvious. In addition, pre-activation with Mish works slightly better than pre-activation with ReLU.

TABLE IX
EXPERIMENTAL RESULTS OF VERIFYING THE OPERATIONS OR OPERATION SEQUENCES. "ReLU" AND "MISH" INDICATE THE ACTIVATION FUNCTION USED IN THE U-NET BLOCK, "P" REPRESENTS PRE-ACTIVATION, AND "IN" MEANS ADDING INSTANCE NORMALIZATION.

No.	Experiments	F1-score	AUROC
1	U-Net-ReLU	0.8191	0.9863
2	U-Net-Mish	0.7921	0.9801
3	U-Net-IN-ReLU	0.8288	0.9882
4	U-Net-ReLU(P)	0.8260	0.9881
5	U-Net-Mish(P)	0.7920	0.9797
6	U-Net-IN-Mish	0.8284	0.9879
7	U-Net-IN-ReLU(P)	0.8294	0.9882
8	U-Net-IN-Mish(P)	0.8296	0.9884
9	Genetic U-Net	0.8314	0.9885

Some of the above observations, or patterns found from the evolutionary results have the potential to be summarized as important knowledge base to be used to further improve our future work.

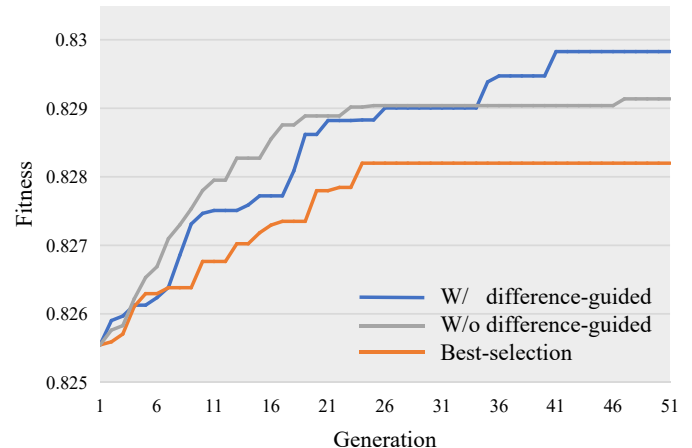


Fig. 8. Evolutionary trajectories in three different situations.

D. Ablation Study

Difference-guided crossover: To verify the effect of utilizing the difference-guided crossover, we compare the performances of the algorithms while searching with and without the difference-guided crossover. We conduct this experiment with the same initial population and other settings for both algorithms. We obtain the statistics of the mean value of fitness of the best five individuals in the population of each generation. As shown in Fig. 8, it is noticeable that the difference-guided crossover can improve the search ability of the algorithm and help to get better results, especially, in the final phase.

Environmental selection: To keep the convergence of the algorithm and at the same time maintain the population diversity, we adopt a selection scheme integrating deterministic and random selection. Here we demonstrate the benefits of this scheme by comparing it with the best-selection. The experiments are conducted with the same initial population and other settings. Fig. 8 also clearly reveals the advantage of the proposed selection scheme. The best-selection results in the algorithm getting poor performance because of premature convergence.

VI. CONCLUSION

In this paper, a novel method of neural architecture search (NAS) for retinal vessel segmentation, named Genetic U-Net, is proposed based on the U-shaped encoder-decoder structure, where the existing methods of retinal vessel segmentation can hardly make further improvements. Genetic U-Net evolves a model that outperforms existing mainstream methods in retinal vessel segmentation. In addition, the searched architecture achieves a significant reduction in the computational complexity, memory demand, and execution time, which indicates that the searched architecture can be more easily deployed for clinical applications. Furthermore, we find that utilizing some simple operations in the building blocks of the model can greatly boost the performance in vessel segmentation, which are considered as very useful knowledge base extracted for our future work. We expect that the proposed approach of NAS can be extended to other related applications, such as pavement crack segmentation or semantic segmentation of urban scenes.

ACKNOWLEDGMENT

This work was supported by the Key Lab of Digital Signal and Image Processing of Guangdong Province, by the Key Laboratory of Intelligent Manufacturing Technology (Shantou University), Ministry of Education, by the Science and Technology Planning Project of Guangdong Province of China under grant (180917144960530, 2019A050519008, 2019A050520001), by the State Key Lab of Digital Manufacturing Equipment & Technology under grant DMETKF2019020, and by the National Defense Technology Innovation Special Zone Projects.

REFERENCES

- [1] M. M. Fraz, P. Remagnino, A. Hoppe, B. Uyyanonvara, A. R. Rudnicka, C. G. Owen, and S. A. Barman, "Blood vessel segmentation methodologies in retinal images—a survey," *Computer methods and programs in biomedicine*, vol. 108, no. 1, pp. 407–433, 2012.
- [2] P. Vostatek, E. Claridge, H. Uusitalo, M. Hauta-Kasari, P. Fält, and L. Lensu, "Performance comparison of publicly available retinal blood vessel segmentation methods," *Computerized Medical Imaging and Graphics*, vol. 55, pp. 2–12, 2017.
- [3] I. P. Chatziralli, E. D. Kanonidou, P. Kerytopoulos, P. Dimitriadis, and L. E. Papazisis, "The value of fundoscopy in general practice," *The open ophthalmology journal*, vol. 6, p. 4, 2012.
- [4] M. D. Abràmoff, M. K. Garvin, and M. Sonka, "Retinal imaging and image analysis," *IEEE reviews in biomedical engineering*, vol. 3, pp. 169–208, 2010.
- [5] L. D. Hubbard, R. J. Brothers, W. N. King, L. X. Clegg, R. Klein, L. S. Cooper, A. R. Sharrett, M. D. Davis, J. Cai, A. R. in Communities Study Group *et al.*, "Methods for evaluation of retinal microvascular abnormalities associated with hypertension/sclerosis in the atherosclerosis risk in communities study," *Ophthalmology*, vol. 106, no. 12, pp. 2269–2280, 1999.
- [6] M. Ortega, M. G. Penedo, J. Rouco, N. Barreira, and M. J. Carreira, "Personal verification based on extraction and characterisation of retinal feature points," *Journal of Visual Languages & Computing*, vol. 20, no. 2, pp. 80–90, 2009.
- [7] C. Simon, "A new scientific method of identification," *New York state journal of medicine*, vol. 35, no. 18, pp. 901–906, 1935.
- [8] Q. Jin, Z. Meng, T. D. Pham, Q. Chen, L. Wei, and R. Su, "Dunet: A deformable network for retinal vessel segmentation," *Knowledge-Based Systems*, vol. 178, pp. 149–162, 2019.
- [9] O. Ronneberger, P. Fischer, and T. Brox, "U-net: Convolutional networks for biomedical image segmentation," in *International Conference on Medical image computing and computer-assisted intervention*. Springer, 2015, pp. 234–241.
- [10] M. Z. Alom, C. Yakopcic, M. Hasan, T. M. Taha, and V. K. Asari, "Recurrent residual u-net for medical image segmentation," *Journal of Medical Imaging*, vol. 6, no. 1, p. 014006, 2019.
- [11] B. Wang, S. Qiu, and H. He, "Dual encoding u-net for retinal vessel segmentation," in *International Conference on Medical Image Computing and Computer-Assisted Intervention*. Springer, 2019, pp. 84–92.
- [12] X. Xiao, S. Lian, Z. Luo, and S. Li, "Weighted res-unet for high-quality retina vessel segmentation," in *2018 9th International Conference on Information Technology in Medicine and Education (ITME)*. IEEE, 2018, pp. 327–331.
- [13] J. Long, E. Shelhamer, and T. Darrell, "Fully convolutional networks for semantic segmentation," in *Proceedings of the IEEE conference on computer vision and pattern recognition*, 2015, pp. 3431–3440.
- [14] Z. Yan, X. Yang, and K.-T. Cheng, "Joint segment-level and pixel-wise losses for deep learning based retinal vessel segmentation," *IEEE Transactions on Biomedical Engineering*, vol. 65, no. 9, pp. 1912–1923, 2018.
- [15] Y. Wu, Y. Xia, Y. Song, D. Zhang, D. Liu, C. Zhang, and W. Cai, "Vessel-net: retinal vessel segmentation under multi-path supervision," in *International Conference on Medical Image Computing and Computer-Assisted Intervention*. Springer, 2019, pp. 264–272.
- [16] L. Mou, L. Chen, J. Cheng, Z. Gu, Y. Zhao, and J. Liu, "Dense dilated network with probability regularized walk for vessel detection," *IEEE transactions on medical imaging*, vol. 39, no. 5, pp. 1392–1403, 2019.
- [17] T. Laibacher, T. Weyde, and S. Jalali, "M2u-net: Effective and efficient retinal vessel segmentation for real-world applications," in *Proceedings of the IEEE Conference on Computer Vision and Pattern Recognition Workshops*, 2019, pp. 0–0.
- [18] M. Sandler, A. Howard, M. Zhu, A. Zhmoginov, and L.-C. Chen, "Mobilenetv2: Inverted residuals and linear bottlenecks," in *Proceedings of the IEEE conference on computer vision and pattern recognition*, 2018, pp. 4510–4520.
- [19] O. Russakovsky, J. Deng, H. Su, J. Krause, S. Satheesh, S. Ma, Z. Huang, A. Karpathy, A. Khosla, M. Bernstein *et al.*, "Imagenet large scale visual recognition challenge," *International journal of computer vision*, vol. 115, no. 3, pp. 211–252, 2015.
- [20] B. Zoph, V. Vasudevan, J. Shlens, and Q. V. Le, "Learning transferable architectures for scalable image recognition," in *Proceedings of the IEEE conference on computer vision and pattern recognition*, 2018, pp. 8697–8710.
- [21] B. Zoph and Q. V. Le, "Neural architecture search with reinforcement learning," *arXiv preprint arXiv:1611.01578*, 2016.
- [22] B. Baker, O. Gupta, N. Naik, and R. Raskar, "Designing neural network architectures using reinforcement learning," *arXiv preprint arXiv:1611.02167*, 2016.
- [23] L. Xie and A. Yuille, "Genetic cnn," in *Proceedings of the IEEE international conference on computer vision*, 2017, pp. 1379–1388.

- [24] Z. Lu, I. Whalen, V. Boddeti, Y. Dhebar, K. Deb, E. Goodman, and W. Banzhaf, "Nsga-net: neural architecture search using multi-objective genetic algorithm," in *Proceedings of the Genetic and Evolutionary Computation Conference*, 2019, pp. 419–427.
- [25] H. Liu, K. Simonyan, and Y. Yang, "Darts: Differentiable architecture search," in *International Conference on Learning Representations*, 2018.
- [26] A. Brock, T. Lim, J. M. Ritchie, and N. J. Weston, "Smash: One-shot model architecture search through hypernetworks," in *6th International Conference on Learning Representations*, 2018.
- [27] Q. Yu, D. Yang, H. Roth, Y. Bai, Y. Zhang, A. L. Yuille, and D. Xu, "C2fnas: Coarse-to-fine neural architecture search for 3d medical image segmentation," in *Proceedings of the IEEE/CVF Conference on Computer Vision and Pattern Recognition*, 2020, pp. 4126–4135.
- [28] C. Liu, L.-C. Chen, F. Schroff, H. Adam, W. Hua, A. L. Yuille, and L. Fei-Fei, "Auto-deeplab: Hierarchical neural architecture search for semantic image segmentation," in *Proceedings of the IEEE conference on computer vision and pattern recognition*, 2019, pp. 82–92.
- [29] G. Ghiasi, T.-Y. Lin, and Q. V. Le, "Nas-fpn: Learning scalable feature pyramid architecture for object detection," in *Proceedings of the IEEE conference on computer vision and pattern recognition*, 2019, pp. 7036–7045.
- [30] H. Xu, L. Yao, W. Zhang, X. Liang, and Z. Li, "Auto-fpn: Automatic network architecture adaptation for object detection beyond classification," in *Proceedings of the IEEE International Conference on Computer Vision*, 2019, pp. 6649–6658.
- [31] N. Wang, Y. Gao, H. Chen, P. Wang, Z. Tian, C. Shen, and Y. Zhang, "Nas-fcos: Fast neural architecture search for object detection," in *Proceedings of the IEEE/CVF Conference on Computer Vision and Pattern Recognition*, 2020, pp. 11 943–11 951.
- [32] Z. Zhu, C. Liu, D. Yang, A. Yuille, and D. Xu, "V-nas: Neural architecture search for volumetric medical image segmentation," in *2019 International Conference on 3D Vision (3DV)*. IEEE, 2019, pp. 240–248.
- [33] D. Yang, H. Roth, Z. Xu, F. Milletari, L. Zhang, and D. Xu, "Searching learning strategy with reinforcement learning for 3d medical image segmentation," in *International Conference on Medical Image Computing and Computer-Assisted Intervention*. Springer, 2019, pp. 3–11.
- [34] A. Mortazi and U. Bagci, "Automatically designing cnn architectures for medical image segmentation," in *International Workshop on Machine Learning in Medical Imaging*. Springer, 2018, pp. 98–106.
- [35] Y. Weng, T. Zhou, Y. Li, and X. Qiu, "Nas-unet: Neural architecture search for medical image segmentation," *IEEE Access*, vol. 7, pp. 44 247–44 257, 2019.
- [36] S. Kim, I. Kim, S. Lim, W. Baek, C. Kim, H. Cho, B. Yoon, and T. Kim, "Scalable neural architecture search for 3d medical image segmentation," in *International Conference on Medical Image Computing and Computer-Assisted Intervention*. Springer, 2019, pp. 220–228.
- [37] X. Glorot and Y. Bengio, "Understanding the difficulty of training deep feedforward neural networks," in *Proceedings of the thirteenth international conference on artificial intelligence and statistics*, 2010, pp. 249–256.
- [38] Y. Bengio, P. Simard, and P. Frasconi, "Learning long-term dependencies with gradient descent is difficult," *IEEE transactions on neural networks*, vol. 5, no. 2, pp. 157–166, 1994.
- [39] Z. Wang, N. Zou, D. Shen, and S. Ji, "Non-local u-nets for biomedical image segmentation," in *Proceedings of the AAAI Conference on Artificial Intelligence*, 2020.
- [40] S. Guan, A. A. Khan, S. Sikdar, and P. V. Chitnis, "Fully dense unet for 2-d sparse photoacoustic tomography artifact removal," *IEEE journal of biomedical and health informatics*, vol. 24, no. 2, pp. 568–576, 2019.
- [41] Z. Gu, J. Cheng, H. Fu, K. Zhou, H. Hao, Y. Zhao, T. Zhang, S. Gao, and J. Liu, "Ce-net: Context encoder network for 2d medical image segmentation," *IEEE transactions on medical imaging*, vol. 38, no. 10, pp. 2281–2292, 2019.
- [42] K. He, X. Zhang, S. Ren, and J. Sun, "Deep residual learning for image recognition," in *Proceedings of the IEEE Conference on Computer Vision and Pattern Recognition (CVPR)*, June 2016, pp. 770–778.
- [43] G. Huang, Z. Liu, L. Van Der Maaten, and K. Q. Weinberger, "Densely connected convolutional networks," in *Proceedings of the IEEE conference on computer vision and pattern recognition*, 2017, pp. 4700–4708.
- [44] C. Szegedy, W. Liu, Y. Jia, P. Sermanet, S. Reed, D. Anguelov, D. Erhan, V. Vanhoucke, and A. Rabinovich, "Going deeper with convolutions," in *Proceedings of the IEEE conference on computer vision and pattern recognition*, 2015, pp. 1–9.
- [45] V. Nair and G. Hinton, "Rectified linear units improve restricted boltzmann machines vinod nair," vol. 27, 06 2010, pp. 807–814.
- [46] D. Misra, "Mish: A self regularized non-monotonic neural activation function," *arXiv preprint arXiv:1908.08681*, 2019.
- [47] D. Ulyanov, A. Vedaldi, and V. Lempitsky, "Instance normalization: The missing ingredient for fast stylization," *arXiv preprint arXiv:1607.08022*, 2016.
- [48] S. Ioffe and C. Szegedy, "Batch normalization: Accelerating deep network training by reducing internal covariate shift," *arXiv preprint arXiv:1502.03167*, 2015.
- [49] G. Lin and X. Yao, "Analysing crossover operators by search step size," in *Proceedings of 1997 IEEE International Conference on Evolutionary Computation (ICEC'97)*. IEEE, 1997, pp. 107–110.
- [50] B. L. Miller, D. E. Goldberg *et al.*, "Genetic algorithms, tournament selection, and the effects of noise," *Complex systems*, vol. 9, no. 3, pp. 193–212, 1995.
- [51] J. H. Holland *et al.*, *Adaptation in natural and artificial systems: an introductory analysis with applications to biology, control, and artificial intelligence*. MIT press, 1992.
- [52] Y. Leung, Y. Gao, and Z.-B. Xu, "Degree of population diversity—a perspective on premature convergence in genetic algorithms and its markov chain analysis," *IEEE Transactions on Neural Networks*, vol. 8, no. 5, pp. 1165–1176, 1997.
- [53] M. Zbigniew, "Genetic algorithms+ data structures= evolution programs," *Computational Statistics*, pp. 372–373, 1996.
- [54] D. E. Goldberg and J. H. Holland, "Genetic algorithms and machine learning," 1988.
- [55] K. He, X. Zhang, S. Ren, and J. Sun, "Delving deep into rectifiers: Surpassing human-level performance on imagenet classification," in *Proceedings of the IEEE international conference on computer vision*, 2015, pp. 1026–1034.
- [56] M. Zhang, J. Lucas, J. Ba, and G. E. Hinton, "Lookahead optimizer: k steps forward, 1 step back," in *Advances in Neural Information Processing Systems*, 2019, pp. 9597–9608.
- [57] D. P. Kingma and J. Ba, "Adam: A method for stochastic optimization," *arXiv preprint arXiv:1412.6980*, 2014.
- [58] T.-Y. Lin, P. Goyal, R. Girshick, K. He, and P. Dollár, "Focal loss for dense object detection," in *Proceedings of the IEEE international conference on computer vision*, 2017, pp. 2980–2988.
- [59] J. Staal, M. D. Abràmoff, M. Niemeijer, M. A. Viergever, and B. Van Ginneken, "Ridge-based vessel segmentation in color images of the retina," *IEEE transactions on medical imaging*, vol. 23, no. 4, pp. 501–509, 2004.
- [60] C. G. Owen, A. R. Rudnicka, R. Mullen, S. A. Barman, D. Monekosso, P. H. Whincup, J. Ng, and C. Paterson, "Measuring retinal vessel tortuosity in 10-year-old children: validation of the computer-assisted image analysis of the retina (caiar) program," *Investigative ophthalmology & visual science*, vol. 50, no. 5, pp. 2004–2010, 2009.
- [61] A. Hoover, V. Kouznetsova, and M. Goldbaum, "Locating blood vessels in retinal images by piecewise threshold probing of a matched filter response," *IEEE Transactions on Medical Imaging*, vol. 19, no. 3, pp. 203–210, 2000.
- [62] P. Liskowski and K. Krawiec, "Segmenting retinal blood vessels with deep neural networks," *IEEE transactions on medical imaging*, vol. 35, no. 11, pp. 2369–2380, 2016.
- [63] J. I. Orlando, E. Prokofyeva, and M. B. Blaschko, "A discriminatively trained fully connected conditional random field model for blood vessel segmentation in fundus images," *IEEE transactions on Biomedical Engineering*, vol. 64, no. 1, pp. 16–27, 2016.
- [64] R. Vega, G. Sanchez-Ante, L. E. Falcon-Morales, H. Sossa, and E. Guevara, "Retinal vessel extraction using lattice neural networks with dendritic processing," *Computers in biology and medicine*, vol. 58, pp. 20–30, 2015.
- [65] Q. Li, B. Feng, L. Xie, P. Liang, H. Zhang, and T. Wang, "A cross-modality learning approach for vessel segmentation in retinal images," *IEEE transactions on medical imaging*, vol. 35, no. 1, pp. 109–118, 2015.
- [66] Z. Fan, Y. Rong, J. Lu, J. Mo, F. Li, X. Cai, and T. Yang, "Automated blood vessel segmentation in fundus image based on integral channel features and random forests," in *2016 12th World Congress on Intelligent Control and Automation (WCICA)*. IEEE, 2016, pp. 2063–2068.
- [67] Z. Fan and J.-J. Mo, "Automated blood vessel segmentation based on de-noising auto-encoder and neural network," in *2016 International Conference on Machine Learning and Cybernetics (ICMLC)*, vol. 2. IEEE, 2016, pp. 849–856.
- [68] J. Mo and L. Zhang, "Multi-level deep supervised networks for retinal vessel segmentation," *International journal of computer assisted radiology and surgery*, vol. 12, no. 12, pp. 2181–2193, 2017.

VII. APPENDIX

A. Visualization of Searched Architectures

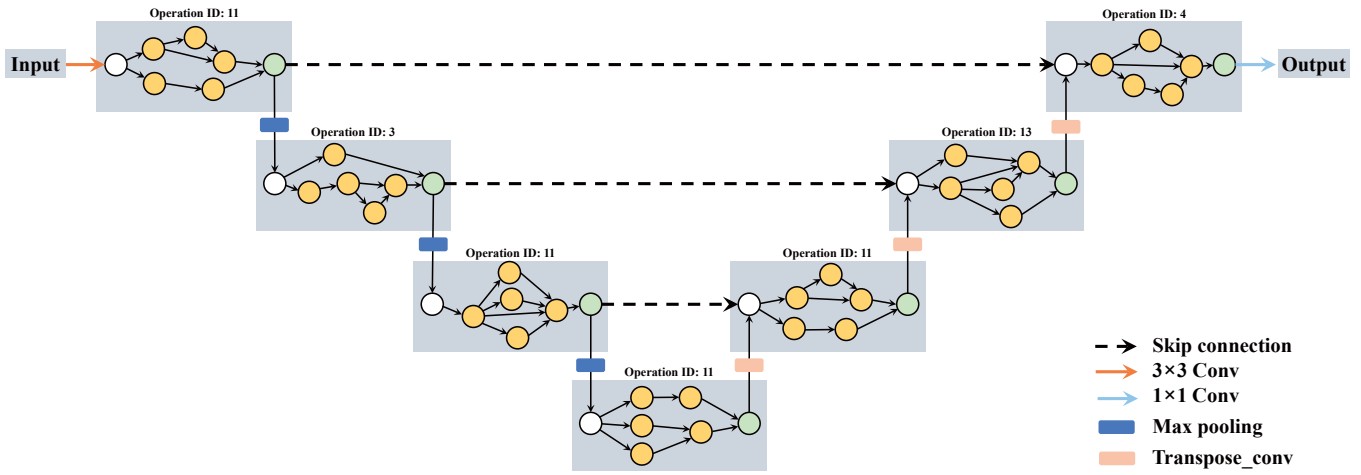


Fig. 9. The first best architecture.

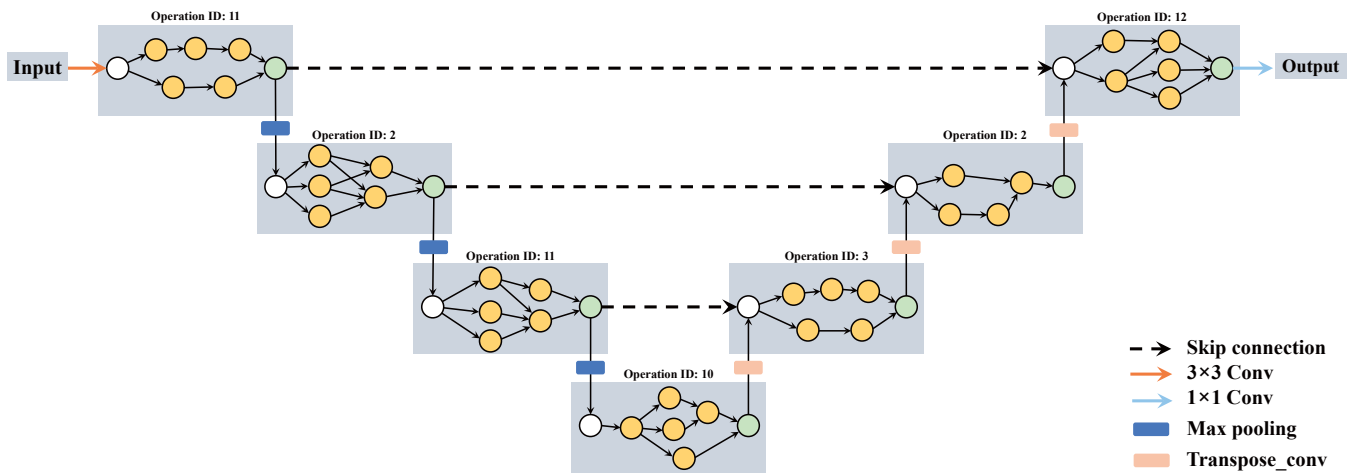


Fig. 10. The second best architecture.

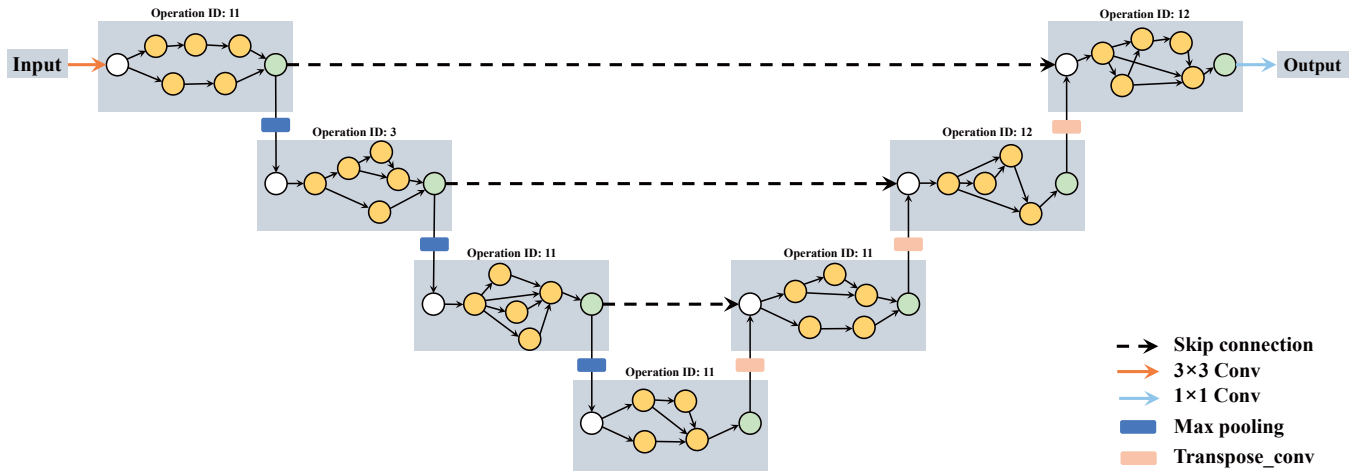


Fig. 11. The third best architecture.

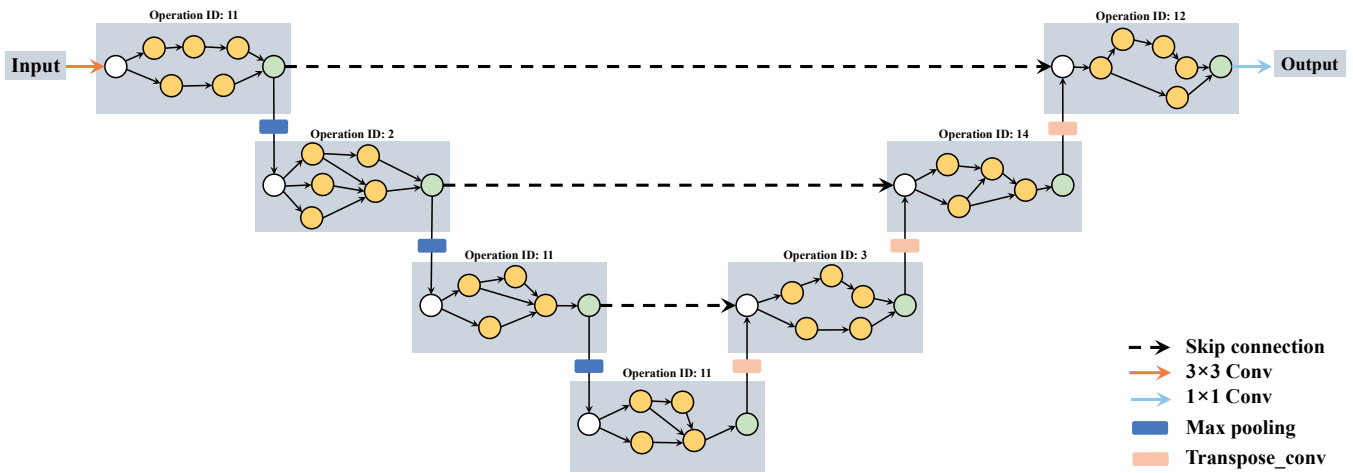


Fig. 12. The fourth best architecture.

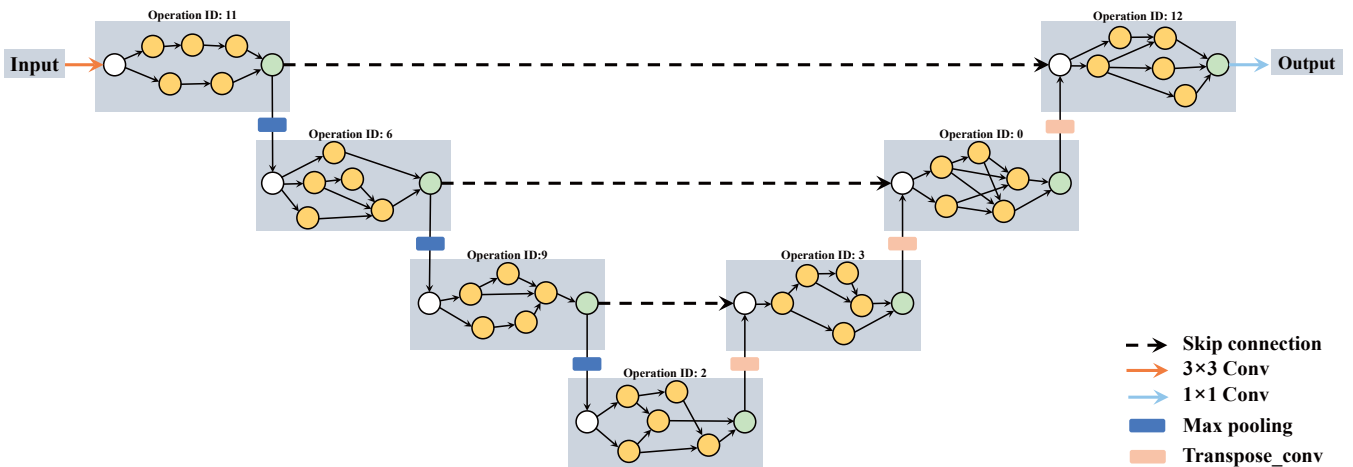


Fig. 13. The fifth best architecture.